J|A|C|S ARTICLES

Published on Web 08/05/2009

Optical Detection of Disordered Water within a Protein Cavity

Robert A. Goldbeck,*,† Marlisa L. Pillsbury,‡ Russell A. Jensen,‡ Juan L. Mendoza,‡ Rosa L. Nguyen,† John S. Olson,§ Jayashree Soman,§ David S. Kliger,† and Raymond M. Esquerra*,‡

Department of Chemistry and Biochemistry, University of California, Santa Cruz, California 95064, Department of Chemistry and Biochemistry, San Francisco State University, San Francisco, California 94132, and Department of Biochemistry and Cell Biology and the W. M. Keck Center for Computational Biology, Rice University, Houston, Texas 77005

Received April 27, 2009; E-mail: goldbeck@chemistry.ucsc.edu; esquerra@sfsu.edu

Abstract: Internal water molecules are important to protein structure and function, but positional disorder and low occupancies can obscure their detection by X-ray crystallography. Here, we show that water can be detected within the distal cavities of myoglobin mutants by subtle changes in the absorbance spectrum of pentacoordinate heme, even when the presence of solvent is not readily observed in the corresponding crystal structures. A well-defined, noncoordinated water molecule hydrogen bonded to the distal histidine (His64) is seen within the distal heme pocket in the crystal structure of wild type (wt) deoxymyoglobin. Displacement of this water decreases the rate of ligand entry into wt Mb, and we have shown previously that the entry of this water is readily detected optically after laser photolysis of MbCO complexes. However, for L29F and V68L Mb no discrete positions for solvent molecules are seen in the electron density maps of the crystal structures even though His64 is still present and slow rates of ligand binding indicative of internal water are observed. In contrast, time-resolved perturbations of the visible absorption bands of L29F and V68L deoxyMb generated after laser photolysis detect the entry and significant occupancy of water within the distal pockets of these variants. Thus, the spectral perturbation of pentacoordinate heme offers a potentially robust system for measuring nonspecific hydration of the active sites of heme proteins.

Introduction

Internal water molecules important to protein structure and function may be highly conserved in homologous protein families, much as are key amino acid residues.[1] The fundamental roles played by water molecules in internal protein cavities in satisfying the H-bonding potentials of main chain atoms in turns, coils, and loops, determining the stability and rigidity of proteins, shifting the pK_a values of buried ionizable residues, and modulating dynamic processes such as folding, catalysis, and proton transfers are driving an emerging need for reliable methods for detecting internal hydration.[2−9] However, traditional structural techniques remain limited in this regard. The electron densities of buried water molecules are frequently obscured in X-ray diffraction studies by positional disorder, and the NMR detection of internal water is often limited by orientational disorder and short residence times.[10−12] Consequently, detection of internal water molecules within a given protein has tended to be incomplete and inconsistent between methods. This situation has prompted an increasing reliance on computational methods to search for the less ordered and more rapidly exchanging water molecules missed by current experimental approaches and has left open to controversy fundamental questions such as the extent to which water may be buried in the apolar cavities of proteins.[9,13]

We have been focusing on the extent and functional effects of hydration of the heme pocket of myoglobin and have developed an experimental method that uses a convenient marker provided by the visible absorption bands of the pentacoordinate, high spin form of the iron(II) porphyrin cofactor to detect the entry of water after laser photolysis of carbon monoxide. We find that this optical method reliably and quantitatively detects the entry of internal (noncoordinated) water into the distal pockets of a series of Mb mutants after photodissociation of ligands.[14−16] This detection appears to be unaffected by positional disorder, allowing us to "see" the presence of water molecules in deoxyMb variants, even when discrete electron density for internal water is not visible in the crystal structure. These results imply that it may be possible to

† University of California.
‡ San Francisco State University.
§ Rice University.

(1) Teeter, M. M. *Annu. Rev. Biophys. Biophys. Chem.* **1991**, *20*, 577–600.
(2) Park, S.; Saven, J. G. *Proteins* **2005**, *60*, 450–463.
(3) Takano, K.; Funahashi, J.; Yamagata, Y.; Fujii, S.; Yutani, K. *J. Mol. Biol.* **1997**, *74*, 132–142.
(4) Mao, Y.; Ratner, M. A.; Jarrold, M. F. *J. Am. Chem. Soc.* **2000**, *122*, 2950–2951.
(5) Schutz, C. N.; Warshel, A. *Proteins* **2002**, *44*, 400–417.
(6) Cheung, M. S.; Garcia, A.; Onuchic, J. N. *Proc. Natl. Acad. Sci. U.S.A.* **2002**, *99*, 685–690.
(7) Meyer, E. *Protein Sci.* **1992**, *1*, 1543–1562.
(8) Hofacker, I.; Schulten, K. *Proteins* **1998**, *30*, 100–107.
(9) Damjanović, A.; Schlessman, J. L.; Fitch, C. A.; García, A. E.; García-Moreno, E. B. *Biophys. J.* **2007**, *93*, 2791–2804.
(10) Phillips, G. N.; Pettitt, B. M. *Protein Sci.* **1995**, *4*, 149–158.
(11) Zhang, X. J.; Matthews, B. W. *Protein Sci.* **1994**, *3*, 1031–1039.
(12) Denisov, V. P.; Halle, B. *J. Am. Chem. Soc.* **1994**, *116*, 10324–10325.
(13) Imai, T.; Hiraoka, R.; Kovalenko, A.; Hirata, F. *Proteins* **2007**, *66*, 804–813.

generalize optical methods for internal water detection to other chromophore-containing protein cavities, either natural or engineered. Cao et al.[17] carried out similar photolysis experiments with Mb(FeIII)NO complexes and observed water penetration into the protein by monitoring the appearance of the intense 409 nm Soret band that is due to water coordination with the ferric iron atom. Rates for water entry ($\sim 10^5$ M^{-1} s^{-1}) and NO escape ($\sim 5 \times 10^6$ s^{-1}) after photolysis were determined and are similar to those measured in our MbCO photolysis experiments, adding validity to our analyses of the smaller spectral changes associated with noncoordinated water entry into the distal pocket of unliganded ferrous Mb.[14,15]

The noncoordinated water molecule present in the distal pocket of wild-type deoxyMb is functionally important in decreasing the bimolecular rate for ligand entry into the protein and lowering the overall affinity of the protein for ligands. This slowing of ligand association is proportional to $(1 - n_w)$, where n_w is the fractional occupancy of the water molecule in the distal pocket. The value of n_w is $\sim$0.8 for the wild-type protein.[14,18−24] This internal water molecule is readily detected in the crystal structure of wild-type deoxyMb. However, no electron density attributable to water has been reported in the crystal structures of the L29F and V68L myoglobin mutants,[25−27] even though these mutants react slowly with ligands when compared to variants containing apolar or "dry" distal pockets (i.e., H64A, H64V, H64L, and H64F deoxyMb).[28]

An NMR study by La Mar et al. found qualitative evidence for high occupancy of distal water near the glutamine side chain in H64Q Mb, another mutant that reacts relatively slowly with ligands.[29] There are no electron density peaks attributable to distal pocket water in the crystal structure of H64Q deoxyMb, but we were able to detect its presence after photolysis of Gln64 MbCO by using our spectral assay.[14] The amide side chain of glutamine is highly polar and water penetration was expected; however, at least four different positions are possible in which the water could be donating or accepting a hydrogen bond from the terminal O and NH_2 atoms of the Gln side chain, which itself is highly mobile. Thus, we attributed the lack of discrete water electron density to a high degree of disorder. Building on this previous work, we have further tested the generality of the optical spectrokinetic assay of deoxyMb hydration by examining the distal pockets of six additional Mb mutants. V68L and L29F Mb were chosen because they retain His64 but appear to have little or no crystallographically detectable water. L29W and L29F/V68L Mb were examined to see if the decrease in distal pocket volume would reduce or eliminate water penetration. H64L/L29F Mb was examined as a control to see if the benzyl side chain of Phe29 influenced the spectrokinetic properties of deoxyMb, and H64L/V68N Mb was examined to see if the amide side chain would facilitate water penetration into Mb containing Leu64. The results are compelling and indicate that the rapid deoxyheme spectral changes, which occur after laser photodissociation of MbCO, do provide a robust, independent method for detecting hydration of the ligand binding site in globins, even when positional disorder occurs.

Scheme 1

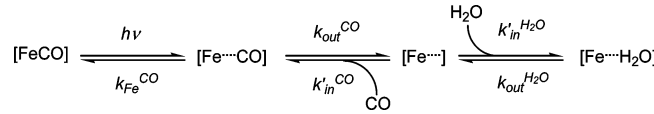

Experimental Procedures

Recombinant sperm whale Mb mutants were cloned, expressed, and purified as described previously.[27] Experimental conditions and data analysis were as described by Goldbeck et al.[14] Time-resolved optical absorption (TROA) data were collected in the heme visible band spectral region by using a broadband probe light source and multichannel detection after photolysis excitation with a frequency-doubled Nd:YAG laser (8 ns, 40 mJ pulses). MbCO samples with concentrations of $\sim$70 μM were photolyzed in 1 cm path length cells sealed under 1 atm of CO. We used singular value decomposition (SVD), a model independent method for analyzing two-dimensional data, to decompose the array of photolysis difference absorption spectra versus time delay data into orthogonal spectral and temporal basis vectors ranked by the magnitudes of their overall contributions.[30] The two largest SVD components were used as inputs to a kinetic modeling procedure that explicitly included microscopic rate constants for water entry and exit from the distal heme pocket as well as for geminate and bimolecular ligand recombination after CO photolysis, as described previously.[14,21]

A complete description of the model is given in Goldbeck et al.,[14] and the chemical reaction scheme is given in Scheme 1. The second SVD component represents the difference between the [Fe···H_2O] deoxyMb species and the initial anhydrous photoproduct, [Fe···]. The fitting analysis provides values for all parameters in Scheme 1 using time courses associated with components one (geminate bimolecular CO recombination, Figure 2, right panels, red traces) and two (water entry and displacement by CO, Figure 2, right panels, blue traces). The equilibrium water occupancy values, n_w, were calculated from the ratio of the fitted water entry,

(14) Goldbeck, R. A.; Bhaskaran, S.; Ortega, C.; Mendoza, J. L.; Olson, J. S.; Soman, J.; Kliger, D. S.; Esquerra, R. M. *Proc. Natl. Acad. Sci. U.S.A.* **2006**, *103*, 1254–1259.
(15) Esquerra, R. M.; Goldbeck, R. A.; Kim-Shapiro, D. B.; Kliger, D. S. *Biochemistry* **1998**, *37*, 17527–17536.
(16) Esquerra, R. M.; Bhaskaran, S.; Pillsbury, M. L.; Mendoza, J. L.; Jensen, R. A.; Lintner, B.; Kliger, D. S.; Goldbeck, R. A. *J. Biol. Chem.* **2008**, *283*, 14165–14175.
(17) Cao, W.; Christian, J. F.; Champion, P. M.; Rosca, F.; Sage, J. T. *Biochemistry* **2001**, *40*, 5728–5737.
(18) Rohlfs, R. J.; Mathews, A. J.; Carver, T. E.; Olson, J. S.; Springer, B. A.; Egeberg, K. D.; Sligar, S. G. *J. Biol. Chem.* **1990**, *265*, 3168–3176.
(19) Smerdon, S. J.; Dodson, G. G.; Wilkinson, A. J.; Gibson, Q. H.; Blackmore, R. S.; Carver, T. E.; Olson, J. S. *Biochemistry* **1991**, *30*, 6252–6260.
(20) Olson, J. S.; Phillips, G. N. *J. Biol. Chem.* **1996**, *271*, 17593–17596.
(21) Olson, J. S.; Phillips, G. N. *J. Biol. Inorg. Chem.* **1997**, *2*, 544–552.
(22) Scott, E. E.; Gibson, Q. H.; Olson, J. S. *J. Biol. Chem.* **2001**, *276*, 5177–5188.
(23) McNaughton, L.; Hernández, G.; LeMaster, D. M. *J. Am. Chem. Soc.* **2003**, *125*, 3813–3820.
(24) Dantsker, D.; Roche, C.; Samuni, U.; Blouin, G.; Olson, J. S.; Friedman, J. M. *J. Biol. Chem.* **2005**, *280*, 38740–38755.
(25) Schotte, F.; Lim, M.; Jackson, T. A.; Smirnov, A. V.; Soman, J.; Olson, J. S.; Phillips, G. N.; Wulff, M.; Anfinrud, P. A. *Science* **2003**, *300*, 1944–1947.
(26) Schotte, F.; Soman, J.; Olson, J. S.; Wulff, M.; Anfinrud, P. A. *J. Struct. Biol.* **2004**, *147*, 235–246.
(27) Quillin et al. did not detect significant distal pocket water occupancy in the deoxy V68L Mb crystal structure, but nevertheless did note that unassigned electron density near the distal histidine may have been due to distal water present in a minor protein conformation rotating Leu68 away from the heme iron atom: Quillin, M. L.; Li, T.; Olson, J. S.; Phillips, G. N.; Dou, Y.; Ikeda-Saito, M.; Regan, R.; Carlson, M.; Gibson, Q. H.; Li, H.; Elber, R. *J. Mol. Biol.* **1995**, *245*, 416–436.
(28) Carver, T. E.; Brantley, R. E.; Singleton, E. W.; Arduini, R. M.; Quillin, M. L.; Phillips, G. N.; Olson, J. S. *J. Biol. Chem.* **1992**, *267*, 14443–14450.
(29) La Mar, G. N.; Dalichow, F.; Zhao, X.; Dou, Y.; Ikeda-Saito, M.; Chiu, M. L.; Sligar, S. G. *J. Biol. Chem.* **1994**, *269*, 29629–29635.
(30) Henry, E. R.; Hofrichter, J. *Methods Enzymol.* **1992**, *210*, 129–192.

Table 1. Summary of Crystal Parameters, Refinement, and Model Statistics for H64L/V68N Met- and DeoxyMb

	mutant myoglobin (PDB ID)	
	H64L/V68N metMb (PDB code 3H58)	H64L/V68N deoxyMb (PDB code 3H57)
unit cell parameters:		
a b c (Å)	90.13 90.13 45.26	90.32 90.32 45.23
α β γ (deg)	90 90 120	90 90 120
refinement and model statistics		
resolution range	40−1.8	45−1.7
number of reflections (total/free)	19 536/953	22 079/1026
R_{merge} (overall/outer shell)	0.035/0.066	0.045/0.088
completeness (overall/ outer shell)	99.7/99.2	96.6/87.4
mean $\langle I\rangle/\langle\sigma(I)\rangle$	18.9	23.8
R_{cryst} (R_{free})	0.196 (0.219)	0.214 (0.233)
rmsd bonds (Å)	0.01	0.01
rmsd angles (deg)	1	1.4
average *B* factor (Å^2)	17.8	16.8
number of water molecules	212	222
Ramachandran plot, residues in		
most favorable region (%)	98.0	98.0
additional allowed region (%)	2.0	2.0
generously allowed region (%)	0.0	0.0
disallowed region (%)	0.0	0.0

$k_{in}^{H_2O}[H_2O]$, and exit, $k_{out}^{H_2O}$, rate constants, which defines the equilibrium constant for partitioning water into the distal pocket, $K_{partition}^{H_2O}$ (i.e., $n_w = K_{partition}^{H_2O}/(1 + K_{partition}^{H_2O})$). These rate constants were obtained by fitting the observed absorbance changes associated with water entry (reflected mainly in the V_2 SVD component) to the differential equations prescribed by the reactions in Scheme 1. The intrinsic water entry difference spectra for the Mb mutants examined in the present study were constrained to be similar, when scaled to 100% occupancy, to that previously calculated for wild-type Mb.[14]

Determination of the Crystal Structures of H64L/V68N Met- and DeoxyMb. Crystals for H64L/V68N met- and deoxyMb were prepared as described previously for recombinant Mbs with Asn at position 122 and were of space group *P*6.[31] Diffraction data were collected at cryogenic temperatures on an RAXIS IV++ detector and RUH3R rotating anode at 100 K using 10 min 0.5 deg frames. Data were processed with d*trek,[32] and all structures were refined using CNS starting from the known structure of the wild-type protein.[33] Relevant statistics are given in Table 1.

Results

Overview of CO Rebinding Data. The spectrokinetic method for determining n_w takes advantage of a small spectral shift in the Fe(II)−porphyrin visible absorption bands upon the entry of water into the distal heme pocket after CO photolysis. The amplitude of this spectral signal correlates with the fraction of water occupancy, n_w, in the equilibrium deoxyMb structure.[14,15] Because the amplitude of this water signal is small as compared to that of the heme Fe−CO bond photolysis difference spectrum at most wavelengths, the absorbance changes associated with water entry are not immediately obvious in the time-resolved optical absorbance (TROA) photolysis spectra reported for the MbCO variants in Figure 1. However, the appearance of this signal can be discerned directly by carefully examining the long wavelength region of the difference spectra for the MbCO complexes with a polar ligand binding site and modest geminate recombination yields, for example, wild-type, L29F, L29F/V68L, and V68L Mb (Figure 1A,B,E,F). In these cases, the positive spectral extremum near 600 nm shows a slight growing in of amplitude on the geminate recombination time scale, ∼0.5 μs, despite the loss of amplitude from the concurrent geminate rebinding process. The spectrokinetics generated by SVD analysis (see Figure 2) for these four variants are the most qualitatively similar of the 7 Mbs examined.

In general, the spectral data in Figure 1 represent a wide range of kinetic behavior with respect to geminate recombination yields on the 10^{-8} to 10^{-6} s time scale and bimolecular recombination on the 10^{-5} to 10^{-3} s time scale. This diversity can obscure comparisons based on qualitative indicators of distal pocket water entry (Table 2). In particular, the higher geminate recombination yields of L29F/H64L (expected to be anhydrous) and H64L/V68N (expected to facilitate water penetration) MbCO, Figure 1C and G, respectively, both produced sufficient decay of the CO photolysis difference spectrum on short time scales to obscure water entry based simply on evolution of the 600 nm extremum. In contrast, no geminate recombination occurs for L29W MbCO (Figure 1D), and the time scale for bimolecular recombination to this mutant was extended by 2 orders of magnitude as compared to that for wild-type MbCO, demonstrating as previously observed that steric intrusion by Trp29 greatly hinders the access of both water and ligands to the distal pocket (Table 2).[34b,35]

The two highest ranked SVD basis spectra (U_1 and U_2) and their time evolutions (V_1 and V_2) shown in Figure 2 provide a more quantitative look at the water entry and ligand rebinding signals for each of the variants.[36] The first component of each variant corresponds mainly to its geminate and bimolecular CO rebinding processes. The spectral signal for water entry after CO photolysis was evident principally in the second SVD component, shown in blue in Figure 2a−g. In the mutants with significant distal water occupancy, L29F, V68L, L29F/V68L, and H64L/V68N, the second component (Figure 2b,i; f,m; e,l, and g,n, respectively) had a spectral shape and time evolution similar to that observed for the entry of water into the distal pocket of wild-type Mb (Figure 2a,h). This difference spectrum corresponded to a small blue shift of the deoxy visible band near 560 nm and additional small changes near 540 and 600 nm that were complete by ∼1 μs.[14] In particular, the normalized amplitude of the L29F deoxyMb signal was ∼60% of that observed for the wild type.[37]

Fitting to the kinetic model of Goldbeck et al.[14] for the competition between geminate and bimolecular CO recombination and heme pocket hydration yielded a water occupancy value, $n_w = k_{in}^{H_2O}[H_2O]/(k_{in}^{H_2O}[H_2O] + k_{out}^{H_2O})$, of 0.5 for L29F Mb

(31) Phillips, G. N., Jr.; Arduini, R. M.; Springer, B. A.; Sligar, S. G. *Proteins* **1990**, *7*, 358–65.
(32) Pflugrath, J. W. *Acta Crystallogr.* **1999**, *D55*, 1718–1725.
(33) Brunger, A. T.; Adams, P. D.; Clore, G. M.; Delano, W. L.; Gros, P.; Grosse-Kunstleve, R. W.; Jiang, J.-S.; Kuszewski, J.; Nilges, M.; Pannu, N. S.; Read, R. J.; Rice, L. M.; Simonson, T.; Warren, G. L. *Acta Crystallogr.* **1998**, *D54*, 905–921.
(34) (a) Nienhaus, K.; Ostermann, A.; Nienhaus, G. U.; Parak, F. G.; Schmidt, M. *Biochemistry* **2005**, *44*, 5095–5105. (b) Schmidt, M.; Nienhaus, K.; Pahl, R.; Krasselt, A.; Anderson, S.; Parak, F.; Nienhaus, G. U.; Srajer, V. *Proc. Natl. Acad. Sci. U.S.A.* **2005**, *102*, 11704–11709.
(35) Hirota, S.; Li, T.; Phillips, G. N., Jr.; Olson, J. S.; Mukai, M.; Kitagawa, T. *J. Am. Chem. Soc.* **1996**, *118*, 7845–7846.
(36) The $\mathbf{V}_i$ vectors were weighted by their singular values S_i (obtained from the SVD of the data matrix $\mathbf{A} = \mathbf{USV}^T$, where $\mathbf{U} = [U_1U_2U_3, ...U_m]$, $\mathbf{V} = [V_1V_2V_3, ...V_n]$, and the diagonal elements of the diagonal matrix **S** are S_1, S_2, S_3, ...S_n) and normalized to the initial weighted amplitude of the first component, $S_1V_{1,1} \equiv S_1V_1(t_1)$, to permit comparison between the variants independently of experimental differences in sample concentration, path length, and photolysis yield.
(37) The normalized spectrokinetic amplitude of this signal was taken as the (peak−trough) amplitude of V_2, weighted and normalized as shown in Figure 2.

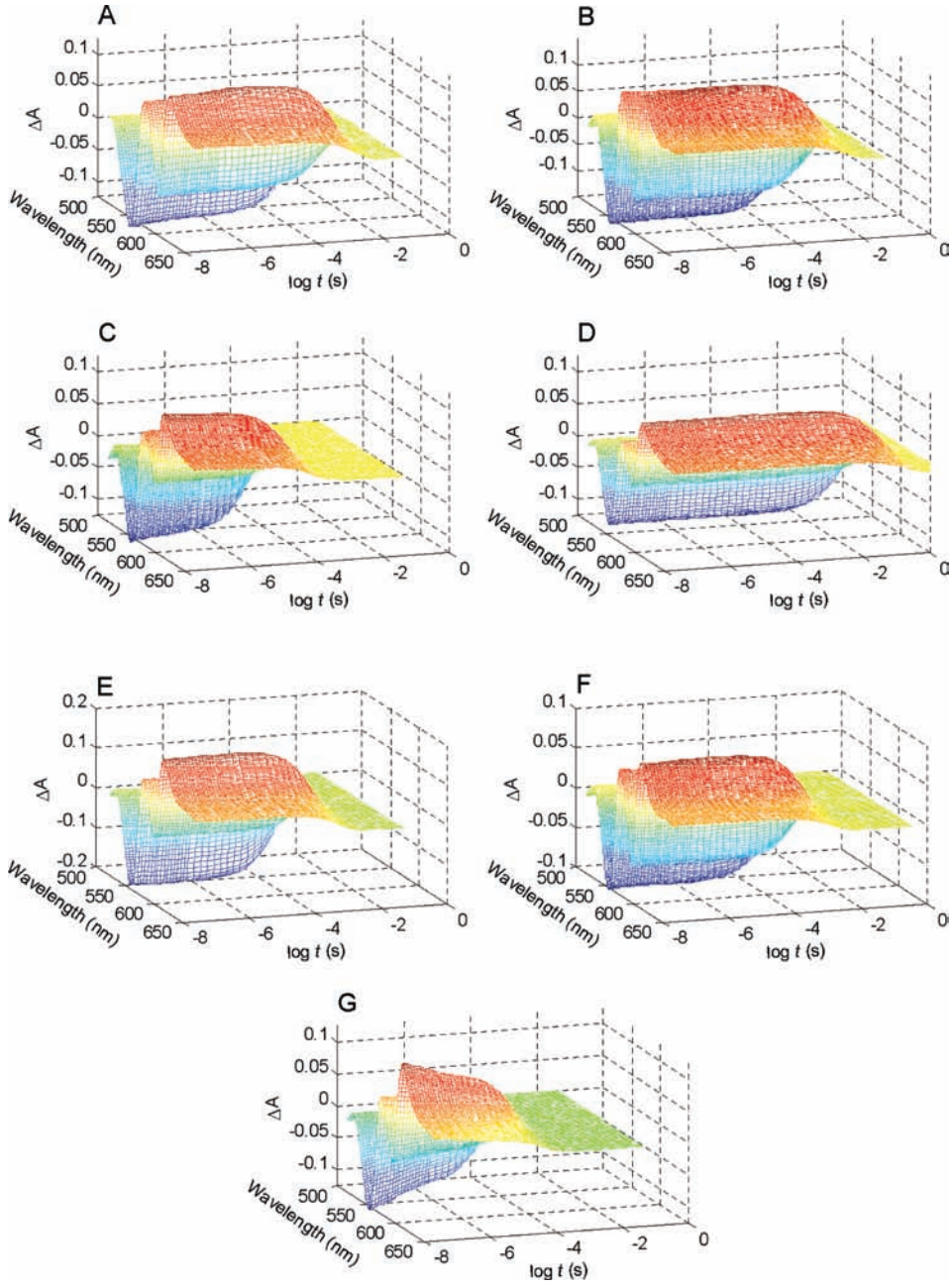

Figure 1. Time-resolved optical absorption spectra of heme visible bands in MbCO variants: (A) wild type, (B) L29F, (C) L29F/H64L, (D) L29W, (E) L29F/V68L, (F) V68L, and (G) H64L/V68N.

(Table 2), which was, as expected, 60% of the wild-type occupancy. The goodness of the fit to the data provided by this model can be seen in the comparisons between the time evolution data and the calculated evolutions for the species studied (Figure 2h−n). The expression for the observed ligand association rate constant derived from this model, $k' = (1 - n_w)\phi_g k_{in}^{CO}$, where $\phi_g = k_{Fe}^{CO}/(k_{out}^{CO} + k_{Fe}^{CO})$ is the geminate recombination yield,[14] also gave good agreement with the observed rate constants obtained by fitting a simple exponential to the slow, millisecond phase for bimolecular rebinding (k'[CO] column, Table 2).

Disordered Water in L29F and V68L DeoxyMb. Spectral detection of water in the distal pocket of L29F Mb ($n_w \approx 0.5$, Figure 2b, Table 2) was initially surprising. Previous picosecond time-resolved X-ray crystallographic studies found evidence for the entry of water into the wild-type protein after CO photolysis but not the mutant.[25,26] Schotte et al.[26] suggested that the greater intrusion of Phe29 into the heme pocket as compared to that of the wild-type leucine residue after CO escape could block water entry and explain the lack of water in the distal pocket observed in the equilibrium crystal structure of the mutant. However, the large size of the second spectral component in the SVD analysis in Figure 2b suggests strongly that water is present. The simplest interpretation is that the large benzyl side chain prevents the noncoordinated water molecule from localizing at a single well-ordered position that is hydrogen bonded to His64 as in the wild-type protein, thus spreading the ~50% water occupancy over a distribution of positions within the mutant distal pocket. The rms translational variation of the water molecule in the mutant cavity must be larger than the X-ray detection limit,

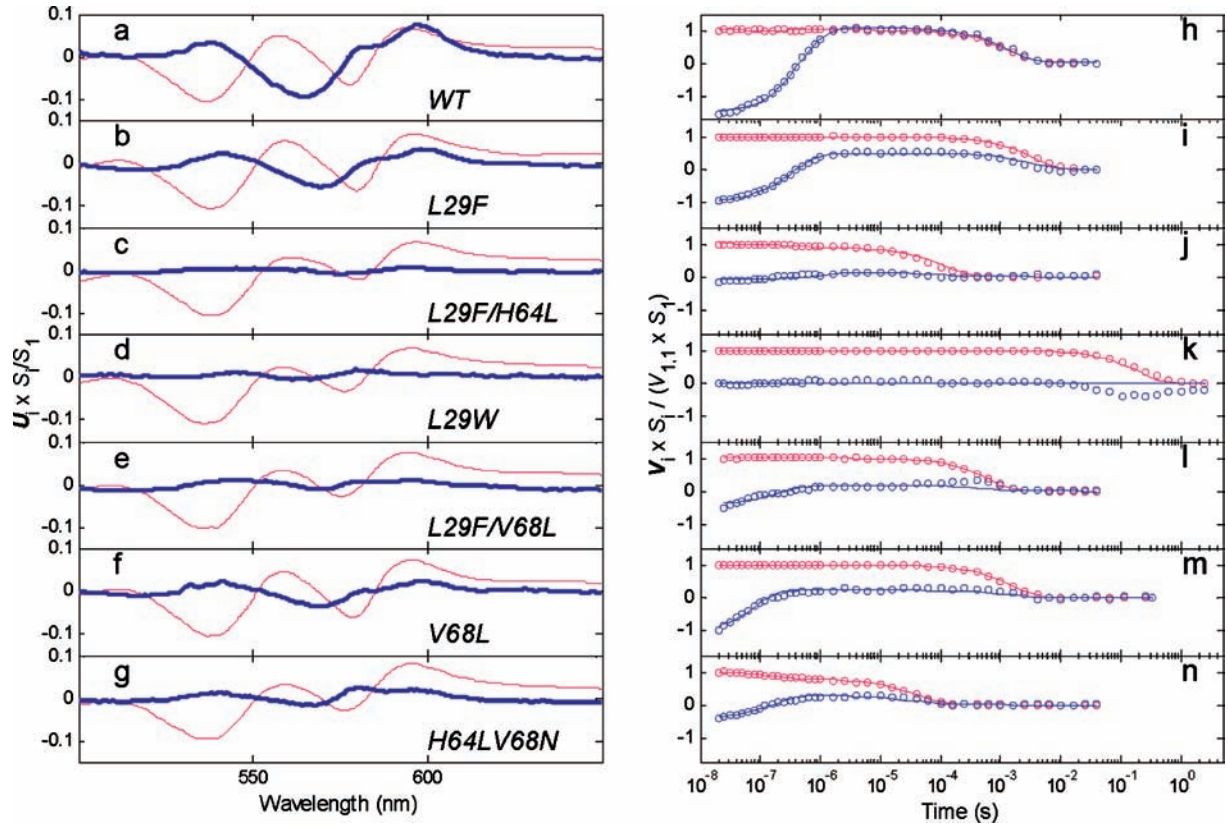

Figure 2. First two SVD components of time-resolved photolysis difference spectra (red and blue, respectively) for (a−g) scaled spectral basis vectors U_1 and $20 \times U_2S_2/S_1$ and (h−n) scaled temporal basis vectors $V_1/V_{1,1}$ and $25 \times V_2S_2/(V_{1,1}S_1)$ (where $V_{1,1} \equiv V_1(t_1)$) for the MbCO mutants: (a,h) wild type, (b,i) L29F, (c,j) L29F/H64L, (d,k) L29W, (e,l) L29F/V68L, (f,m) V68L, and (g,n) H64L/V68N. The scalings applied to the U_1, U_2, V_1, and V_2 components observed for the MbCO variants were chosen to facilitate size comparisons of their distal pocket water signals, which to a good approximation were represented by the second basis vectors, U_2 and V_2. (U_2 is highlighted in bold for each species.) The singular value scaling described above for the orthonormal V_i vectors (with V_2 further scaled by a factor of 25 for clarity) permits an approximate indication of the relative water signal sizes from the peak to trough amplitudes of the scaled V_2 components shown in panels h−n. The solid lines in panels h−n show fits to the V_i data points calculated from the hydration kinetic model of ref 14 with the parameter values (e.g., n_w) shown in Table 2.

Table 2. Kinetic Parameters for Wild-Type MbCO and Variants L29F, L29W, H64L, V68L, L29F/H64L, and L29F/V68L[a]

variant	k_{Fe}^{CO} (μs^{-1})	$k_{in}^{CO}[CO]^c$ (μs^{-1})	k_{out}^{CO} (μs^{-1})	$k_{in}^{H_2O}[H_2O]$ (μs^{-1})	$k_{out}^{H_2O}$ (μs^{-1})	n_w	X-ray structure, H_2O occupancy: deoxyMb (metMb)	ϕ_g	$1 - n_w$	$k'[CO]^e$ (μs^{-1})	τ_{obs}^{-1} (μs^{-1})
WT[b]	0.11	(0.08)	2.2	9.0	1.7	0.84	0.84 (0.99)	0.051	0.16	0.00064	0.00066
L29F	0.053	0.032	2.6	34	31	0.52	0.00 (1.00)	0.020	0.48	0.00031	0.00031
L29W[f]				(0.08)	(1)[g]	≤0.07	n.d.		0.93		3.4×10^{-6}
H64L[b]	2.0	0.078	2.2			0	0.00 (0.00)	0.48	1	0.037	0.040
V68L	0.62	0.028	13	32	35	0.48	0.36 (1.00)	0.044	0.52	0.00064	0.00065
L29F/H64L	0.32	(0.08)	(2.2)[d]	(0.07)	(0.6)[h]	≤0.12	n.d.	0.13	0.88	0.009	0.012
L29F/V68L	1.1	0.078	34	26	49	0.35	n.d.	0.032	0.65	0.0016	0.0015
H64L/V68N	1.7	0.15	4.7	160	240	0.39	0.43 (1.00)	0.27	0.61	0.025	0.023

[a] Rate constants and inverse lifetimes reported in μs^{-1}; [CO] = 1.0 mM; $[H_2O]$ = 55.5 M. [b] From ref 14. [c] Constrained during fitting procedure to a maximum (diffusion-controlled) value of 0.08 μs^{-1}. [d] Constrained to a minimum value of 2.2 μs^{-1} (value from ref 14 for wild type and H64L Mb). [e] $k' \equiv (1 - n_w)\phi_g k_{in}^{CO}$. [f] The ϕ_g value of L29W MbCO was too small to be determined from our data and was approximated in the n_w analysis by constraining k_{Fe}^{CO} to the wild-type value and k_{out}^{CO} to the geminate escape rate constant reported in ref 34, ~(5 ns)$^{-1}$, a procedure that led to a fitted value of 0.011 μs^{-1} for $k_{in}^{CO}[CO]$. These values were not listed in the table because they could not be determined uniquely here, due to the lack of a significant geminate recombination phase. [g] Not defined, constrained to 1 μs^{-1}, could be much larger, but the ratio $k_{in}^{H_2O}[H_2O]/k_{out}^{H_2O}$ is defined to be <0.1. [h] Not defined, could be much larger, but the ratio $k_{in}^{H_2O}[H_2O]/k_{out}^{H_2O}$ is defined to be <0.1.

~0.5 Å,[10] to account for the lack of discrete electron density (Figure 3, second structure, top row).

An alternative explanation of the deoxyheme spectral signal for L29F Mb is that the multipole of the Phe29 side chain coincidentally induces a shift in the deoxyheme absorption spectrum similar to that of water entry. To test this possibility, we examined the double mutant L29F/H64L Mb, in which the distal histidine was replaced by leucine. The imidazole side chain of His64 fixes the position of the internal water molecule by hydrogen-bond formation. Replacement of His64 with Leu leads to complete loss of water from the distal pocket as measured by the spectrokinetic assay or crystallography (Figure 4, left panels).[38] Thus, if the signal seen for the single L29F mutant were due to the phenyl ring, it should also be seen for the L29F/H64L double mutant; however, if the L29F Mb signal is due to disordered water partially stabilized by the polarity of His64, it should be

(38) Quillin, M. L.; Arduini, R. M.; Olson, J. S.; Phillips, G. N. *J. Mol. Biol.* **1993**, *234*, 140–155.

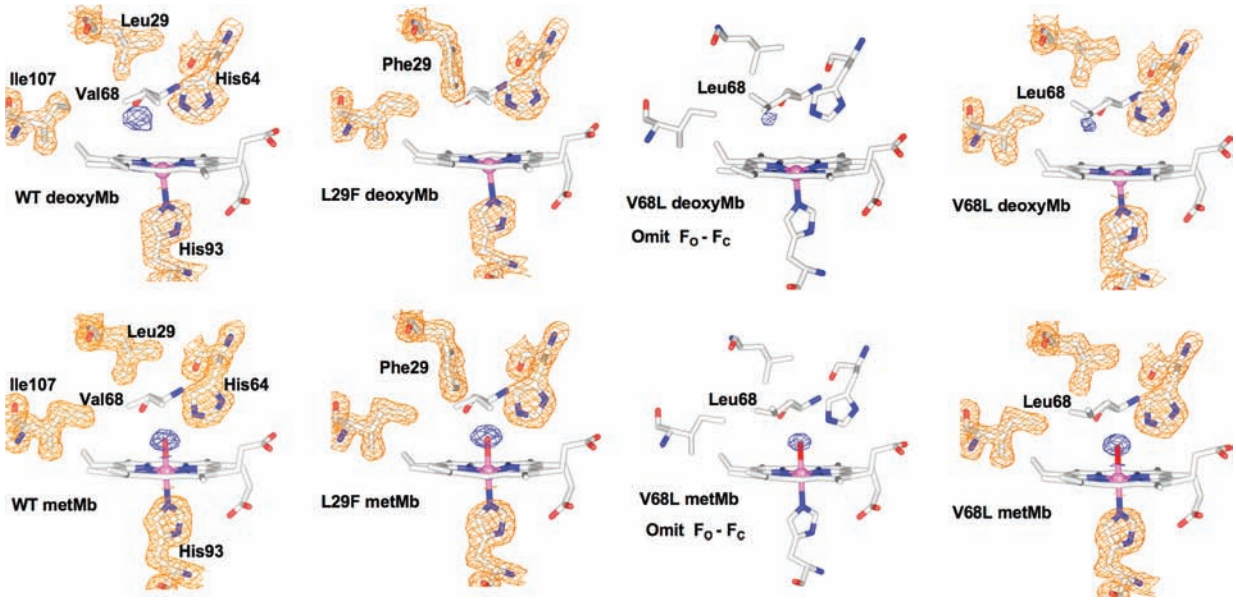

Figure 3. Electron densities for the distal pocket residues, noncoordinated and coordinated water, and the proximal histidine in the deoxygenated (Fe^{2+}) and met (Fe^{3+}) forms of wild-type (2MGL, 2MBW), V68L (1MLR, 1MLS), and L29F (1MOA, 2SPM) recombinant sperm whale Mb. Occupancies for the water electron density (shown in blue) are given in Table 1. The $2F_O - F_C$ maps for wt deoxy and metMb and V68L metMb were taken from Quillin et al.[27] The final $2F_O - F_C$ maps (upper right structure) for V68L deoxyMb were obtained from a rerefinement of the structure reported by Quillin et al. modeling a water in the small electron density reported in the distal pocket near His64.[27] As part of this refinement, a simulated annealing omit map using $(F_O - F_C)\alpha_C$ coefficients without water in the model was constructed (third structure, top row of Figure 3). In this map, only electron density not associated with the active site amino acids is shown and confirms a small peak above the iron atom, which we modeled with a water in the final structure. For comparison, a simulated annealing, omit map was also constructed for the V68L metMb, using a model without coordinated water. As expected, the electron density peak is significantly larger and clearly assignable to bound water. The $2F_O - F_C$ maps for L29F were taken from Carver et al.[28] When we tried to rerefine these data for L29F deoxyMb, we were unable to "find" water peaks in any of the maps examined, and the final model does not contain water in the distal pocket.

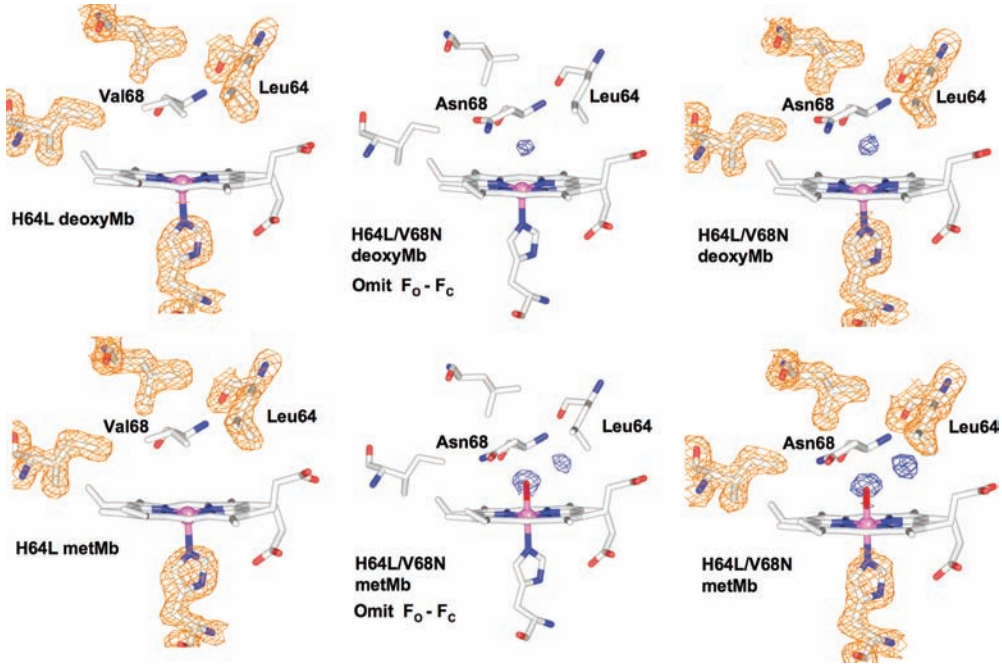

Figure 4. Electron densities for the distal pocket residues, noncoordinated and coordinated water, and the proximal histidine in the deoxygenated (Fe^{2+}) and met (Fe^{3+}) forms of H64L (2MGD, 2MGE) and H64L/V68N (3H57, 3H58) recombinant sperm whale Mb. Occupancies for the water electron density (shown in blue) are given in Table 2. The $2F_O - F_C$ maps for wt deoxy and metMb were taken from Quillin et al.[27] The structures of the double mutant were determined for this work. The middle column contains simulated annealing omit maps calculated using $(F_O - F_C)\alpha_C$ coefficients without any distal pocket water in the model. The final deposited model and structure factors with distal pocket water included were used to construct the $2F_O - F_C$ map in the last column (PDB codes: 3H58, 3H57).

absent for the L29F/H64L double mutant. The results in Figure 2c are clear; there is little or no second SVD component after photolysis of L29F/H64L MbCO ($n_w \leq 0.1$ for the second component, Table 2). Thus, the signal for the single L29F mutant appears to be due to significant water penetration that cannot be detected by crystallography.

Blocking Water Penetration by Filling the Distal Cavity. The original explanation for the lack of crystallographically detectable water in L29F deoxyMb was steric exclusion by the large phenyl side chain, which occupies space adjacent to His64 and partially fills the distal cavity. To explore this idea, we examined L29W and L29F/V68L Mb. The large indole side chain in Trp29 Mb is expected to exclude water from occupying any space near the heme chromophore, and adding a larger amino acid to the 68 position in the presence of Phe29 should also decrease the accessible pocket volume.[34] As shown in Figure 2d,e, both mutations significantly decrease the amplitude of the SVD component associated with water penetration (Figure 2a,b). The signal for L29W was barely detectable, even though nanosecond geminate rebinding is effectively zero and bimolecular rebinding is very slow. The fitted value of n_w for L29W deoxyMb is ≤ 0.1.[39] A signal for L29F/V68L Mb was detected, but n_w is significantly smaller than that for the single L29F mutant (Figure 2b,e, Table 2). These data show that sterically reducing the size of the distal pocket can lead to exclusion of water, but that Phe29 by itself is not large enough to prevent water penetration.

The polar nature of the distal pocket in L29F Mb can be judged by the presence of coordinated water in the ferric form of the mutant. In wt Mb, water is found in both the ferrous and the ferric crystal structures of the unliganded protein, whereas water is only seen in the ferric form of L29F Mb (Figure 3). In contrast, water is absent in the crystal structures of both H64L deoxy- and metMb (Figure 4).

Leu68 and Asn68 Have Opposite Effects on Water Penetration. Quillin et al.[27] suggested that there was a small peak of electron density associated with a distal pocket water molecule adjacent to His64 in the single V68L mutant, but did not include it in their model. When V68L MbCO was examined in our laser photolysis experiments, a detectable second SVD component was observed (Figure 2f) and indicated a relatively high n_w value of 0.48. As in the case of L29F Mb, the distal pocket of Leu68 Mb contains His64, is polar, and shows a well-defined coordinated water in the ferric form (V68L metMb in Figure 3).

In view of Quillin's comments,[27,40] we re-examined his deposited data for V68L deoxyMb, rerefined the structure, placed a partially occupied water molecule at the same position as in wild-type Mb, and obtained the electron density map shown in Figure 3 (upper panel, last column). A simulated annealing omit map, phased without any distal pocket water in the model, was initially calculated to confirm the presence of water (Figure 3, upper row, third structure). A small peak of electron density is present with a refined occupancy of ~0.3 to 0.4, in rough agreement with the spectrokinetic analysis. Regardless of the exact value, both experiments show that the larger, more flexible Leu68 side chain sterically disrupts water interaction with His64, reducing its occupancy and increasing its disorder. The higher n_w value for L29F Mb suggests that, even though more disorder occurs, the Phe29 side chain appears to be increasing the extent of water occupancy, probably through weak interactions with the phenyl multipole that are similar to those causing water/benzene azeotropes.

Replacing Val68 with Asn has been shown to stabilize water in deoxyMb and reduce the rates and equilibrium constants for ligand binding by donating a second hydrogen bond to the internal solvent molecule.[41] As a further test of our spectral assignments, we examined H64L/V68N Mb to see if the Asn68 side chain could attract a water molecule into the distal pocket of H64L Mb, which by itself is anhydrous as measured by both our spectral analysis and crystallography (Figure 3, Table 2). As shown in Figure 2g, a significant water signal is seen for the double mutant. The Asn68 mutation is able to facilitate water penetration by itself, even with Leu at the distal histidine position, and the calculated value of n_w is ~0.4.

To test this result, we determined the crystal structures of the met- and deoxyMb forms of the H64L/V68N double mutant. The resulting electron density maps are shown in Figure 4 (right panels). The occupancy of the water in H64L/V68N mutant was refined to ~0.4 in deoxyMb, and the two peaks in the metMb structure were refined to ~0.9 for the coordinated water and ~0.6 for the second, more external water located near Thr67 and underneath Leu64 (Figure 4). Again, simulated annealing omit maps were calculated without distal pocket water in the model and show clear evidence for solvent in the distal pocket of the double mutant in both the ferric and the ferrous forms (Figure 4, middle panels). The agreement between the spectrokinetic data and the crystal structure of H64L/V68N deoxyMb is quite good, presumably because there are no steric interactions to prevent direct hydrogen bonding to the Asn68 side chain and cause disorder. These data also demonstrate that the spectrokinetic assay can detect water entry irrespective of which residue, His64 or Asn68, is interacting with the solvent molecule and further support the robustness of this optical method.

Discussion

Origin of the Water-Induced Spectral Change. Christian et al.[42] compared the visible absorption and Fe−His93(F8) vibrational band positions for a series of deoxyMb distal pocket mutants, including the L29F mutant studied here. They attributed an observed 1 cm^{-1} decrease in the proximal Fe−His93 stretching frequencies of apolar His64 mutants to a decrease in the electrostatic influence of the distal water dipole moment on the Fe−His93 bond strength. On the other hand, a 4 nm red shift observed in the deoxyMb visible Q-band and band III absorption peaks of the mutants was attributed to changes in the heme electrostatic environment arising from the distal residues themselves. The wavelength shifts observed in the equilibrium spectra of the apolar His64 mutants relative to wild-type Mb are larger than the shift associated with the entry of a water molecule into the distal pocket of wild-type Mb observed after CO photolysis in our work. This comparison suggests that any equilibrium spectral shift contributed by decreased occupancy of the distal water molecular dipole to the total shift could be obscured by larger contributions coming from the mutation-induced changes.

However, in our assay, we are directly measuring the difference between the anhydrous deoxyMb species generated 9 ns after photolysis ([Fe···], Scheme 1) and the final equilibrium deoxyMb species ([Fe···H_2O], Scheme 1). Most amino acid side chain relaxations appear to occur on more rapid time scales (≤ 1 ns).[43−46] Thus, any large effects due to the mutations should affect both the initial 10 ns intermediate and the final product with distal pocket water in place and cancel

(39) The small evolution observed in the V_2 component of L29W Mb at $\sim 10^{-1}$ s after photolysis appears to be associated with bimolecular CO rebinding rather than water entry.
(40) Quillin, M. L. Ph.D. Dissertation, Rice University, 1994.
(41) Krzywda, S.; Murshudov, G. N.; Brzozowski, A. M.; Jaskolski, M.; Scott, E. E.; Klizas, S. A.; Gibson, Q. H.; Olson, J. S.; Wilkinson, A. J. *Biochemistry* **1998**, *37*, 15896–15907.
(42) Christian, J. F.; Unno, M.; Sage, J. T.; Champion, P. M. *Biochemistry* **1997**, *36*, 11198–11204.

out in our analysis. Ligand rebinding and escape and water penetration occur on the hundreds of nanoseconds and microsecond time scales of our experiments. Thus, transient opening and closing of the distal histidine gate must also be occurring on these time scales, and the kinetics and extent of these motions will be dependent on the nature of the mutation. However, the similarity of the spectra of the intermediates for the H64L/V68N mutant and wt Mb argues against a specific spectral effect due to His64.

Increasing solvent polarity (e.g., benzene → water) blue shifts the heme Soret and visible absorption bands of model heme compounds by several nanometers.[47] These shifts occur in both the strongly allowed Soret and the weakly allowed visible bands, whereas water penetration into the distal pocket of Mb shifts only the visible absorption bands.[14,15] The difficulty in finding an equilibrium experimental model for the distal-water spectral shift suggests that a computational approach, with a Hamiltonian that includes electrostatic interaction matrix elements between the water dipole moment and the heme π-electron transition dipoles and, perhaps, heme quadrupole moments, may be a useful alternative.

Water Penetration Rates and Occupancies. One interesting result in Table 2 is the correlation between lower water occupancy (n_w) and faster rates of water entry and exit ($k_{in}^{H_2O}[H_2O]$, $k_{out}^{H_2O}[H_2O]$). Excluding the values of L29W and L29F/H64L, which are undefined because $n_w \leq 0.1$ (i.e., no water is seen), the H_2O entry and exit rates both increase with decreasing occupancy. Clearly, the distal histidine is part of a strong barrier to water penetration and escape, presumably because it can form strong hydrogen bonds with water through either N_δ, keeping the solvent molecule out of the pocket, or N_ε, keeping the water in the pocket. The latter interaction accounts for the high value of n_w in wild-type Mb. Cao et al.[17] observed a similar increase for the rate of water penetration and coordination to H64G metMb after photolysis of NO, consistent with His64 being a gate to water entry.

Steric interactions with Phe29 appear to impede both His64 interactions, causing 3- and 15-fold increases in the water entry and exit rates, respectively, and a drop in n_w. Similar increases, due presumably to steric clashes with His64, are observed for the single V68L and double L29F/V68L mutants. Increased $k_{in}^{H_2O}[H_2O]$ and $k_{out}^{H_2O}[H_2O]$ values were also observed for H64Q Mb.[14] However, the most convincing proof that His64 is the major barrier to water penetration in wt Mb comes from the marked increases in the rates of water movement observed for the H64L/V68N mutant. In this variant, water is stabilized by the amide group of Asn68, but the Leu64 side chain offers 20−100-fold less resistance to water entry and exit, respectively. Similar results are observed for ligand binding, where His64 confers a much larger barrier to entry than Leu64. Thus, ironically the distal histidine, which stabilizes the internal water, is a large barrier to its entry into the distal pocket.

Correlations between Spectral Measurements and Crystallographic Data. To a first approximation, the n_w values calculated from analysis of the second SVD component correlate well with the water occupancies observed in the corresponding crystal structures for wt Mb and the H64L, V68F, V68L, and H64L/V68N mutants (Table 2).[14] The two major outliers are H64Q and L29F deoxyMb (Table 2).[14] The spectral signals for water penetration are large for both mutants; their distal pockets are clearly polar, as judged by 100% occupancy of coordinated water in the ferric forms (Figures 3 and 4);[14] and the rates of ligand binding to these proteins are slow, indicating significant barriers to ligand entry. The control experiment with H64L/L29F Mb shows that the signal for L29F is not due to polar interactions with the phenyl ring. Complete and greater exclusion of water by the L29W and L29F/V68L mutants, respectively, shows that Phe29 is not large enough to prevent water penetration. Together the results for H64Q and L29F Mb demonstrate that the spectrokinetic assay can detect internal water that is too disordered to be observed in crystal structures. Thus, this method may be applicable for studying the dynamics and energetics of noncoordinated water in the active sites of all heme proteins with a pentacoordinate ferrous state without the requirement for positional order.

Acknowledgment. This work was supported financially by NIH grants EB02056 (D.S.K.), GM52588 (R.M.E.), MD000544 (R.M.E.), GM35649 (J.S.O.), and HL47020 (J.S.O.); Robert A. Welch Foundation Grant C-0612 (J.S.O.); and student fellowships from NIH grant GM08574 (Minority Access to Research Careers) (M.L.P.), the ARCS Foundation (R.A.J.), and the Louis Stokes Alliance for Minority Participation (J.L.M.).

JA903409J

(43) Tian, W. D.; Sage, J. T.; Srajer, V.; Champion, P. M. *Phys. Rev. Lett.* **1992**, *68*, 408–411.
(44) Dantsker, D.; Samuni, U.; Friedman, J. M.; Agmon, N. *Biochim. Biophys. Acta* **2005**, *1749*, 234–251.
(45) Merchant, K. A.; Noid, W. G.; Akiyama, R.; Finkelstein, I. J.; Goun, A.; McClain, B. L.; Loring, R. F.; Fayer, M. D. *J. Am. Chem. Soc.* **2003**, *125*, 13804–13818.
(46) Ishikawa, H.; Kwak, K.; Chung, J. K.; Kim, S.; Fayer, M. D. *Proc. Natl. Acad. Sci. U.S.A.* **2008**, *105*, 8619–8624.
(47) Romberg, R. W.; Kassner, R. J. *Biochemistry* **1982**, *21*, 880–886.